Annales
Geophysicae
Discussions

Open Access

EGU

1   **MMS observations of energetic oxygen ions at the low-latitude duskside magnetopause**

2   **during intense substorms**

3

4   Chen Zeng[1,2], Suping Duan[1], Chi Wang[1,2], Lei Dai[1], Stephen Fuselier[3,4], James Burch[3], Roy

5   Torbert[5], Barbara Giles[6], Christopher Russell[7]

6

7   1 State Key Laboratory of Space Weather, National Space Science Center, Chinese Academy of

8   Sciences, China.

9   2 University of Chinese Academy of Sciences, China.

10   3 Southwest Research Institute, San Antonio, Texas, USA.

11   4 The University of Texas at San Antonio, San Antonio, Texas, USA

12   5 University of New Hampshire, Space Science Center, Durham, New Hampshire, USA

13   6 NASA, Goddard Space Flight Center, Greenbelt, MD, USA.

14   7 University of California Los Angeles,IGPP/EPSS, Los Angeles, California, USA

15

16   Corresponding author: cw@spaceweather.ac.cn, spduan@nssc.ac.cn

17

18   **Abstract**

19   Energetic oxygen ions O^+ (>1keV) observed by the Magnetospheric Multiscale (MMS) satellites

20   at the dusk flank magnetopause during the phase 1a and 1b are investigated. There are 31 dusk

21   flank magnetopause crossing events during intense substorms (AE>500 nT) are identified. These

22   31 events of energetic O^+ at the dusk flank magnetopause include 9 events during the expansion

23   phase and 22 events during the recovery phase of intense substorms. It is noted that 9 events of

24   energetic O^+ ion at the dusk flank magnetopause during intense substorms expansion phase are all

25   under the southward IMF conditions. The number density of energetic O^+ at the dusk flank

26   magnetopause ranges from 0.01 cm^{-3} to 0.2 cm^{-3}. The maximum number density ratio of O^+/H^+ is

27   ~0.055 during intense substorm recovery phase with AE index about 610 nT and under the

28 northward interplanetary magnetic field (IMF). The number density ratio of O^+/H^+ also shows an

29 exponential increase with the IMF By. While IMF Bz seems play a minor role in O^+ abundance at

30 the dusk flank magnetopause during intense substrom. Our observations suggest that energetic

31 oxygen ions play a key role in the mass and energy transferring from the tail to the dayside in the

32 magnetosphere during intense substorms.

33

1. Introduction

35 Single charged oxygen ions in the magnetosphere, O^+, are exclusively from the ionosphere. They

36 are an element in the mass and energy transport in the magnetospheric dynamic process during

37 intense substorms (AE >500 nT), especially during the expansion phase and recovery phase of

38 intense substorms [e.g., Daglis et al., 1991;1996; Duan et al., 2017; Fok et al.,2006; Ohtani et al.,

39 2011; Ono et al.,2009; Nose et al.,2000;Yau et al.,1997;2012]. The number density and energy

40 density of oxygen ions, O^+, significantly increase during the intense substorm expansion phase

41 [e.g., Daglis et al., 1994; Duan et al., 2017; Lennartsson and Shelley, 1986]. Daglis et al. [1991]

42 reported that the energy density of O^+ increased non-linearly with AE indices during substorms.

43 The inductive electric field associated with substorm dipolarization is very significant for

44 accelerating particles in the near-Earth plasma sheet [e.g., Dai et al.,2014;2015; Duan et

45 al.,2011;2016; Lui et al.,1999]. Lennartsson and Shelley [1986] proposed that oxygen ions with

46 energy of less than 17keV/e can provide 50% of the number density in the plasma sheet during

47 activity geomagnetic disturbance. The oxygen ions from the nightside auroral region can rapidly

48 feed in the near-Earth magnetosphere during substorm expansion phase [e.g., Daglis and Axford,

49 1996; Duan et al., 2017; Yu et al., 2013].

50

51 O^+ from the ionosphere can be energized up to tens of keV during intense substorm dipolarizations

52 in the near-Earth plasma sheet of magnetotail [Birn et al.,2013; Duan et al., 2017; Fok,et al., 2006;

53 Nose et al.,2000; Ono et al.,2009; Yau et al., 2012]. The oxygen ions out flowing from the

54 ionosphere with low energy of eV are accelerated to about 500 eV at the high altitude polar region

55 [e. g., Yau and Andre, 1997]. And then they are convected tailward into the lobe and the plasma

56 sheet boundary layer (PSBL). Duan et al. [2017] reported that the oxygen ions from the lobe or the

57 PSBL are efficiently accelerated by the kinetic Alfven eigenmode with significant unipolar electric

58 field and rapidly feed in the near-Earth plasma sheet (NEPS) during intense substorm

59 dipolarizations. These energetic oxygen ions in the NEPS can be injected into the inner

60 magnetosphere and drift westward into the duskside outer magnetosphere [e.g., Ganushkina et al.,

61 2005].

62

63 Oxygen ions decay from the ring current and leaked into the dayside low latitude boundary layer

64 [e.g., Li et al., 1993; Ebihara et al., 2011]. Li et al. [1993] reported that the ring current O^+ with

65 tens of keV energy interacted with the Pc 5 waves and then lost towards the dayside magnetopause.

66 Kim et al. [2005] pointed out that a solar wind dynamic pressure enhancement played a key role in

67 the loss of the ring current particle into the outer magnetosphere. Ebihara et al. [2011] proposed

68 that the field line curvature scattering is more effective in the loss of energetic oxygen ions with its

69 large gyro-radius. These energetic oxygen ions with pitch angle of ~90 degrees can leak into the

70 dayside magnetopause. This process may be the key loss mechanism for the ring current ions.

71

72 The energetic oxygen ions density at the dayside magnetopause is asymmetry distribution and has

73 close relationship with the interplanetary magnetic field and solar wind dynamic pressure [e.g.,

74 Bouhram et al., 2005; Phan et al., 2004]. Bouhram et al. [2005] pointed out that the O^+ density is

75 higher in the duskside than in the dawn side magnetopause. O^+ is the dominant contributor to the

76 mass density 30% on the dusk side in comparison to 3% in the dawnside and 4% near noon. Phan

77 et al. [2004] reported that energetic O^+ with energy larger than 3 keV in the reconnection jets are

78 observed by Cluster at the duskside mid-latitude magnetopause under steady southward

79 interplanetary magnetic field (IMF) conditions. There is ample evidence that magnetospheric ions

80 could participate in the magnetopause reconnection and directly escape along reconnected open

81 field lines [e.g., Sonnerrup et al.,1981; Fuselier et al., 1991,2016; Slapak et al., 2012,2015;Wang et

82 al., 2014; Liu et al., 2015]. [Zong et al., 2001] observed O^+ energy dispersion due to time-of-flight

83 (TOF) effects at the dusk flank magnetopause under southward IMF and it was assumed that O^+

84 was escaping from the ring current along the reconnected field lines during steady reconnection.

85 However, However, Fuselier et al. [1989] reported O^+ from the high latitude ionosphere not

86 associated with any substorm cycle. O^+ from the high latitude ionosphere could form the O^+ rich

87 boundary layer in the low latitude magnetopause. While the reconnection rate is likely reduced by

88   the mass-loading, reconnection is not suppressed at the magnetopause[Fuselier et al. 2019].

89

90   At present, O^+ near the dayside low-latitude magnetopause during substorm expansion phase and

91   recovery phase are still not understood. Previous studies of oxygen ions during substorms are

92   mainly focused on O^+ energizations in the near-Earth plasma sheet in the magnetotail [e.g., Duan

93   et al., 2017; Nose et al., 2000; Ohtani et al., 2011]. We investigate statistical features of energetic

94   oxygen ions at the dusk flank magnetopause and their relations with O^+ in the near-Earth plasma

95   sheet during the intense substorms.

96

97   **2. Data**

98   **2.1 Instrumentation and data**

99   This study uses data from the Magnetospheric Multiscale (MMS) mission. This mission comprises

100   four identical satellites that were launched on 2015 March 13 into an elliptical 28-inclination orbit

101   with perigee around 1.2 R_E and apogee around 12 R_E. The electric field **E** is from the electric

102   double probe (EDP) [*Ergun et al.*, 2016; *Lindqvist et al.*, 2016], and magnetic field **B** is from the

103   Fluxgate Magnetometer (FGM) [*Russell et al.*, 2016]. The plasma data are from the Fast Plasma

104   Investigation (FPI) [*Pollock et al.*, 2016] and the Hot Plasma Composition Analyzer (HPCA)

105   [*Young et al.*, 2016]. The FPI has high time resolution of 0.03 s for electrons and 0.15 s for ions in

106   burst mode and 4.5 s in fast mode. The HPCA provides ion composition (H^+, He^{++}, He^+ and O^+)

107   measurements in the energy range from ~1eV to 40 keV [*Young et al.*, 2016]. Although the HPCA

108   instrument employs radio frequency (RF) unit to artificially reduce the proton fluxes in some areas

109   where the proton fluxes are intense, there still exists a low level of background that affects the O^+

110   fluxes in the magnetosheath. The majority of the O^+ fluxes in the magnetosphere side of the

111   magnetopause are at energies above 1 keV and that band below 1keV visible in the magnetosheath

112   side are observations outside the RF operating range and contamination from high proton fluxes.

113   Due to this contamination, the number density of O^+ with energy above 1keV is considered at the

114   magnetopause in our study. The solar wind parameters, IMF and AE index are available from the

115   OMNI data in CDAweb (http://cdaweb.gsfc.nasa.gov/).The data from the MMS 4 satellite are

116   adopted in our investigation since the data difference from other three spacecraft is negligible.

117

118 **2.2 Energetic O^+ at the dusk flank magnetopause during intense substorms**

119 **2.2.1 Detailed event on 3 October 2015**

120 Figure 1 presents the IMF, solar wind dynamic pressure and AE index during the interval from

121 14:30 UT to 16:30 UT on 3 October 2015. The IMF Bz component is negative during this interval

122 as shown in Figure 1c. The minimum value of the IMF Bz component is about -6.7 nT. The solar

123 wind dynamic pressure is about 2 nPa. It increases sharply at 15:10UT. The maximum solar wind

124 dynamic pressure is about 4 nPa. An intense substorm (AE > 500 nT) occurred under the above

125 IMF and solar wind dynamic pressure. The substorm onset time is about 14:45 UT, when the AE

126 index significantly increases. The maximum value of AE index is ~1000 nT at 15:20 UT.

127

128 Figure 2 shows that MMS 4 encountered the duskside magnetopause region from 15:25:10 to

129 15:36:50 UT during the intense substorm recovery phase on 03 October 2015. This interval is

130 marked by the two vertical blue lines in Figure 1. This intense substorm onset time is around

131 14:45 UT with AE maximum value 1000 nT at 15:20 UT as shown in Figure 1e. During the

132 magnetopause crossing, MMS 4 satellites were located at about (6.0, 8.8, -5.1) Re in GSM as

133 shown in the bottom of Figure 2. From top to bottom, panels 2a and 2b show that the magnetic

134 and electric fields in GSM, respectively. Ion temperature, ion and electron number densities, ion

135 velocity in GSM from FPI are shown in Figure 2c, 2d and 2e, respectively. The omnidirectional

136 electron and ion energy fluxes from FPI are shown in Figure 2g and 2h, respectively. The O^+

137 number density at energies above 1keV is displayed in Figure 1f. The last four panels of Figure 2

138 show the omnidirectional differential fluxes of four individual ion species, H^+, O^+, He^+ and He^{++}

139 measured by HPCA, respectively. The different regions encountered by MMS4 during the interval

140 of 15:00 to 16:00UT are marked by the colored bar at the top of Figure 2, with the magnetosheath

141 shown in orange, the outer magnetosphere shown in blue, and the magnetopause region shown in

142 green. From 15:00:00 to 15:25:10 UT, MMS4 was located in the magnetosheath. This region is

143 characterized by a southward magnetic field, low ion temperatures (a few hundred eV, Figure 2c)

144 with relatively high number densities (on the order of ~20 cm-3, Figure 2d), and stable ion flow

145 speeds of about one hundred km/s. There are also very high fluxes at energies around 100 eV for

146 electrons (Figure 2g) and around 1 keV for ions (Figure2h, also see H^+ fluxes in Figure 2i and

147 He^{++} fluxes in Figure 2l) in the magnetosheath. While the He^+ and O^+ fluxes above 1 keV nearly

148   disappear in the magnetosheath (Figure 2j and 2k). From Figure 2k, the majority of the fluxes at

149   energies below 1keV visible in the magnetosheath are the result of contamination from the high

150   proton fluxes.

151

152   The primary magnetopause crossing from the magnetosheath into the magnetosphere lasted about

153   6 min, from 15:31:20 to 15:36:50 UT. Partial encounters of the magnetopause by MMS4 occurred

154   around 15:43:15, 15:47:10 and 15:53:00UT, respectively. The magnetopause region is identified

155   by particle fluxes and the electromagnetic field. The plasma density and ion temperature at the

156   magnetopause are between the corresponding values of the magnetosphere and the magnetosheath,

157   as shown in Figure 2d and 2c, respectively. The magnetopause region can also be identified by the

158   significant increases in electron fluxes at energies about several hundreds of eV and ion fluxes at

159   energies around ~10 keV, as shown in Figure 2g and 2h, respectively. During the interval from

160   15:25:10 to 15:36:50UT, the Bz rotated from southward to northward and back again several times

161   before finally became northward when MMS 4 entered the magnetosphere. The energetic O^+

162   number density is around 0.02 cm^{-3} within the magnetopause boundary layer as shown in Figure

163   2f.

164

165   After 15:36:50 UT, MMS4 entered the magnetosphere which is identified by the observations of a

166   northward magnetic field (Figure 2a), much lower number plasma densities (on the order of ~1

167   cm^{-3}) with respect to densities in the magnetosheath (Figure 2d), higher ion temperatures (a few

168   thousands of eV), and a small bulk ion flow speed. Higher fluxes at energies around several keV

169   for electrons (Figure 2g) and at energies around ~10 keV for ions (Figure 2h) also indicate that

170   MMS4 was in the magnetosphere. Finally, the presence of He^+ and O^+ at energies about ~10 keV

171   is also used as a marker to verify that MMS4 was in the magnetosphere (Figure 2j and 2k).

172

173   **2.2.2 Statistical 31 events of MMS first Phase 1 observations of energetic O^+ at the dusk**

174   **flank magnetopause crossing during intense substorms(AE>500nT)**

175   Based on the in-situ measurements of the dayside magnetopause processes by MMS satellites in

176   phase 1a and phase 1b, 31 events of the dusk flank magnetopause crossing during intense

177   substorms with AE index larger than 500 nT are selected. In our statistical study, the mean value

178 of the H^+ and O^+ fluxes and their densities are calculated in the magnetopause boundary layer.

179 Correspondingly, the solar wind dynamic pressure and IMF Bz, By and AE index from the OMNI

180 data system was averaged during the magnetopause crossing time interval. The phase of the

181 substorm is determined from the AE index.

182

183 Figure 3 displays the locations projected into the XY_{GSM} plane of 31 events of energetic O^+ at the

184 dusk flank magnetopause during intense substorms. The blue curve line represents the nominal

185 magnetopause, which is obtained by magnetopause model of (Shue et al., 1998)] using the IMF Bz

186 ~ -1.96 nT and solar wind dynamic pressure ~ 2.37 nPa (average for the 31 events). The diamond

187 and circle represent the event at the dusk flank magnetopause during the intense substorm

188 expansion phase and recovery phase, respectively. The O^+ number density and the number density

189 ratios of O^+/H^+ are shown by the color diamond and circle at the corresponding magnetopause

190 location in Figure 3a and 3b, respectively. Among the 31 events of energetic O^+ at the dusk flank

191 magnetopause during intense substorms, there are 9 events that occur .during the expansion phase

192 of intense substorms and 22 events occurring during the recovery phase of intense substorms.

193 These 9 and 22 events are shown in Figure 3 by 9 diamonds and 22 circles, respectively. The

194 maximum number density of energetic O^+ is found during intense substorm recovery phase as

195 presented in Figure 3a. On the other hand, the maximum number density ratio of O^+/H^+ is also

196 found during the recovery phase of an intense substorm as shown by the red circle in Figure 3b.

197

198 Figure 4 presents the relationship between the energetic O^+ at the dusk flank magnetopause and

199 AE index during intense substorms. From top to bottom, panels show that the O^+ and H^+ number

200 density, Figure 4a, the number density ratio of O^+/H^+, Figure 4b, and particle flux ratio of O^+/H^+

201 Figure 4c, respectively. The energy channel range of O^+ and H^+ in the HPCA are the same. The

202 O^+/H^+ number density ratio (n_{O^+} / n_{H^+}) and O^+ /H^+ ratio for fluxes (f_{O^+} /f_{H^+}) at ~1keV (energy

203 range from 987.82 to 1165.21 eV), ~10keV (energy range from 9973.98 to 11765.13 eV), ~20keV

204 (energy range from 19310.05 to 22777.82 eV) and ~35 keV(energy range from 31693.41 to

205 37385.04 eV) are defined as the ratio between mean values of their number densities and fluxes,

206 respectively. Figure 4a shows that the number density of energetic O^+ at the dusk flank

207 magnetopause during intense substorms is in the range from 0.01 cm^{-3} to 0.2 cm^{-3}. The maximum

208   number density value of energetic O^+ at the dusk flank magnetopause during intense substorm

209   expansion phase is presented at the higher AE index ~ 870 nT as displayed in Figure 4a the last

210   right blue circle. While the maximum value of the energetic O^+ number density, the ratio of n_{O^+} /

211   n_{H^+}, and f_{O^+} /f_{H^+} at the dusk flank magnetopause during intense substorm recovery phase are all

212   around AE index 600 nT.

213

214   Figure 5 shows the relationship between the energetic O^+ at the dusk flank magnetopause and the

215   IMF By during intense substorms. The format of the Figure 5 is the same as Figure 4. Figure 5a

216   shows that the O^+ and H^+ number densities increase with IMF By when it is larger than 4 nT. From

217   Figure 5b, the O^+/H^+ number density ratio increase in the IMF By is associated with an

218   exponential growth by a factor 0.07. Based on observations, we can define linear functional

219   dependence between the logarithm of O^+/H^+ number density ratio and IMF By as Eq. (1):

220    $$\log(n\,{O^+}/_{H^+}) = 0.07 * \text{IMF By} - 5.14 \tag{1}$$

221   The dependency is constructed using a linear least squares fit. The O^+/H^+ particle flux ratio at

222   energy about 10keV, 20keV and 30keV also show an obvious exponential increase with IMF By.

223   This dependency is consistent with Welling et al. (2011) simulation results found in the ring

224   current.

225

226   Figure 6 shows the relationship between the energetic O^+ at the dusk flank magnetopause and the

227   IMF Bz during intense substorms. The format of the Figure 6 is the same as Figure 4. Figure 6a

228   and Figure 6b both present that among our 31 events of energetic O^+ near the dusk flank

229   magnetopause, there are 9 events during the expansion phase of intense substorms which are all

230   under the southward IMF conditions, as shown the blue circle in Figure 6. While there are only 6

231   events under the northward IMF, as the right circle with IMF Bz > 0 shown. The maximum

232   number density of energetic O^+ at the dusk flank magnetopause is during the intense substorms

233   recovery phase under the southward IMF. But the maximum ratio of nO^+ / nH^+ at the dusk flank

234   magnetopause is during intense substorm recovery phase under the northward IMF. Comparing

235   with IMF By, IMF Bz seems play a minor role in O^+ abundance at the dusk flank magnetopause

236   during intense substrom.

Annales
Geophysicae
Discussions

237

238   Figure 7 displays the relationship between the energetic O^+ at the dusk flank magnetopause and

239   the solar wind dynamic pressure during intense substorms. The format of the Figure 7 is the same

240   as Figure 4. Figure 7a and 7b both present that the number density of energetic O^+ and the O^+ to

241   H^+ number density ratio at the dusk flank magnetopause during intense substorms have a weak

242   correlation with the solar wind dynamic pressure. The maximum number density of energetic O^+

243   at the dusk flank magnetopause, ~ 0.2 cm^{-3} take place at solar wind dynamic pressure 1.9 nPa

244   during an intense substorm recovery phase. While the maximum O^+ to H^+ number density ratio at

245   the dusk flank magnetopause is around solar wind dynamic pressure 2.5 nPa.

246

247   **3. Discussion**

248   Energetic O^+ with high number density are observed by the MMS satellites at the dusk flank

249   magnetopause during the expansion phases and recovery phases of intense substorms, as displayed

250   in Figure 3a and Figure 4a. The number density of energetic oxygen ions is from 0.01 cm^{-3} to 0.2

251   cm^{-3} at the dusk flank magnetopause during intense substorms. This O^+ number density is larger

252   than the energetic O^+ near the duskside mid-latitude magnetopause observed by Cluster, which

253   was 0.011 to 0.053 cm^{-3} [e.g., Bouhram et al., 2005]. Bouhram et al. [2005] demonstrated that the

254   O^+ number density is much higher in the dusk side than in the dawn side magnetopause. The

255   significantly higher number density of energetic O^+ is obtained from MMS at the dusk flank

256   magnetopause during intense substorms in our paper. There are two reasons for this high number

257   density of energetic O^+. The first is the time interval for the observations. Our observations are

258   during intense substorms expansion phase and recovery phase. Daglis et al. [1991] proposed that

259   energetic O^+ were significantly higher in the near-Earth plasma sheet in the magnetotail after

260   intense substorms onset. The impulsive electric field accompanied by intense substorm

261   dipolarization plays a key role in the energization and sunward transfer of oxygen ions in the

262   duskside of midnight plasma sheet in the magnetotail [e.g., Fok et al., 2006; Nose et al., 2000].

263   These energetic O^+ (tens of keV) can be transported sunward into the low latitude boundary layer.

264   The second reason for the high densities is the locations of the observations. Our observations are

265   near the dusk flank magnetopause. This region is easily accessible by energetic O^+ during intense

266   geomagnetic activity. Phan et al. [2004] pointed out that energetic O^+ were observed with very

267   high number density 0.2-0.3 cm^{-3} in the reconnection jets at the dusk-side mid-latitude

268   magnetopause by Cluster.

269

270   During dynamic periods and intense substorms time, light ions yielded more symmetric patterns in

271   density than heavy ions and O$^+$ patterns in the active plasma sheet are a function of IMF

272   conditions (Winglee and Harnett 2011. Winglee et al. 2005). Welling et al. (2011) used

273   multispecies MHD and the PWOM to drive a ring current model, and found positive By pushing

274   the stronger O$^+$ concentrations toward the duskside at a geocentric distance of about 6.6 R$_E$. This

275   O$^+$ density duskward preference with positive IMF By in the near Earth plasma sheet is similar to

276   our results. It may indicate the dusk flank magenetopause O$^+$ enhancing with IMF By is due to the

277   local time variations of O$^+$ in the near Earth plasma sheet tied to IMF By. While IMF Bz seems

278   play a minor role in O$^+$ abundance at the dusk flank magnetopause during intense substrom. These

279   results show the O$^+$ abundance at the dusk flank magnetopause have a corresponding relation with

280   the O$^+$ in the duskside near Earth plasma sheet during intense substorm.

281

282   Among our 31 events of energetic O$^+$ near the dusk flank magnetopause, there are 9 events during

283   intense substorm expansion phase which are all under the southward IMF, as the blue circle shown

284   in Figure 6b. Hsu, T.‐S., and McPherron, R. L. [2003] found that approximately 60% of all

285   substorms expansion phase are correspond to the northward IMF Bz. But there are only 6 events

286   under the northward IMF in our study. Thus our statistical results demonstrate that the energetic

287   O$^+$ near the dusk flank magnetopause dominated occurring under the southward IMF. Previous

288   research demonstrated that the oxygen ions origin from the aurora region can rapidly feed in the

289   near-Earth plasma sheet in the magnetotail during intense substorms [e.g., Daglis and Axford,

290   1996; Duan et al, 2017; Yu et al., 2013]. Oxygen ions can be efficiently energized in the

291   near-Earth plasma sheet during intense substorm dipolarization [e.g., Duan et al., 2017; Fok et al.,

292   2006; Nose et al., 2000]. Under southward IMF conditions, these energetic oxygen ions can be

293   convected sunward and drift westward. As a result, the energetic O$^+$ arrived near the dusk flank

294   magnetopause during intense substorm expansion phase could participate in the magnetopause

295   reconnection and escape along reconnected field lines, as reported by Wang et al. [2014] and Zong

296 et al. [2001]. But from Fuselise et al. [2019], while the reconnection rate is likely reduced by the

297 mass-loading, reconnection is not suppressed at the magnetopause. Whether these energetic O^+

298 could suppress the intense substorm need further investigation.

299

300 **4.   Summary and conclusions**

301 Using the measurements from FPI, HPCA and FGM on MMS mission during the phase 1a and 1b,

302 we have studied 31 events of the energetic oxygen ions distributions at the dusk flank

303 magnetopause during intense substorm expansion phases and recovery phases. According to the

304 above analysis, we can draw our main conclusions as follows. During intense substorms, the

305 energetic oxygen ions are mainly observed at the dusk flank magnetopause within the substorm

306 recovery phase. In our 31 events of energetic O^+ at the dusk flank magnetopause, there are only 9

307 events during the expansion phase of intense substorms. While there are 22 events during the

308 recovery phase of intense substorms. We find out that 9 events of energetic O^+ at the dusk flank

309 magnetopause during intense substorms expansion phase are all under the southward IMF

310 conditions. The O^+/H^+ number density ratio exponential increase with the IMF By and the

311 maximum number density ratio of oxygen ion to proton is ~0.055 during intense substorm

312 recovery phase. The high energetic O^+ number density at the dusk flank magnetopause during

313 intense substorms is in the range from 0.01 cm^{-3} to 0.2 cm^{-3}. Our observations suggest that

314 energetic oxygen ions are a key indicator in the mass and energy transport from the tail to the

315 dayside in the magnetosphere during intense substorms.

316

317 **Data availability**

318 All data used in this study are publicly accessible. MMS data are available at the MMS Science

319 Data Center (https://lasp.colorado.edu/mms/sdc/public/).The OMNI data can be downloaded from

320 the   NASA   Goddard   Space   Flight   Center   Coordinated   Data   Analysis   Web

321 (CDAWeb:http://cdaweb.gsfc.nasa.gov/).

322

323 **Competing interests**

324 The authors declare that they have no conflict of interest.

325

326 **Author contribution**

327   C. Z. conducted the majority of the data processing, analysis and writing for this study. S.P.D, C.W,

328   L.D and S.F participated in the interpretation of the data and modified this paper. J.B, R.T, B.G

329   and C.R produced the data and controlled the data quality. All the authors discussed the results and

330   commented on the paper.

331

339

340   **References**

341   Birn, J., Thomsen, M. F., and Borovsky, J. E. et al.: Substorm ion injections: Geosynchronous

342   observations and test particle orbits in three-dimensional dynamic MHD fields, J. Geophys. Res.,

343   102, 2325–2341, 1997.

344   Bouhram, M., Klecker, B., Paschmann, G., Haaland, S., Hasegawa, H., Blagau, A., et al. (2005).

345   Survey of energetic O^+ ions near the dayside mid-latitude magnetopause with

346   Cluster. Annales Geophysicae, 23(4), 1281–1294. https://doi.org/10.5194/angeo-23-1281-2005

347   Daglis, I. A., N. P. Paschalidis, E. T. Sarris, W. I. Axford, G. Kremser, B. Wilken, and G.

348   Gloeckler (1991), Statistical features of the substorm expansion phase as observed by

349   AMPTE/CCE spacecraft, in Magnetospheric Substorms, Geophys. Monogr. Ser, vol. 64, edited by

350   J. R. Kan et al., pp. 323–332, AGU, Washington, D. C.

351   Daglis, I. A., & Axford, W. I. (1996). Fast ionospheric response to enhanced activity in geospace:

352   Ion feeding of the inner magnetotail. Journal of Geophysical Research, 101(A3), 5047–5065,

353   doi:10.1029/95JA02592.

354   Daglis, I. A., R. M. Thorne, W. Baumjohann, and S. Orsini (1999), The terrestrial ring current:

355   Origin, formation, and decay, Rev. Geophys., 37, 407, doi:10.1029/1999RG900009.

356   Dai, L., J. R. Wygant, C. A. Cattell, S. Thaller, K. Kersten, A. Breneman, X. Tang, R. H. Friedel,

357   S. G. Claudepierre, and X. Tao (2014), Evidence for injection of relativistic electrons into the

358   Earth's outer radiation belt via intense substorm electric fields, Geophys. Res. Lett., 41, 1133–

359   1141,doi:10.1002/2014GL059228.

360   Dai, L., Wang, C., Duan, S., He, Z., Wygant, J. R., Cattell, C. A.,…Tang, X. (2015). Near-Earth

361   injection of MeV electrons associated with intense dipolarization electric fields: Van Allen Probes

362   observations. Geophysical Research Letters, 42, 6170–6179. https://doi.org/10.1002/

363   2015GL064955.

364   Duan, S. P., Liu, Z. X., Liang, J., Zhang, Y. C., & Chen, T. (2011). Multiple magnetic

365   dipolarizations observed by THEMIS during a substorm. Annales de Geophysique, 29(2), 331–

366   339, doi:10.5194/angeo- 29- 331- 2011.

367   Duan, S. P., L. Dai, C. Wang, J. Liang, A. T. Y. Lui, L. J. Chen, Z. H. He, Y. C. Zhang, and V.

368   Angelopoulos (2016), Evidence of kinetic Alfvén eigenmode in the near-Earth magnetotail during

369   substorm expansion phase, *J. Geophys. Res. Space Physics*, 121, 4316–4330, doi:10.1002/

370   2016JA022431.

371   Duan, S., Dai, L., Wang, C., He, Z., Cai, C., Zhang, Y. C., … Khotyaintsev, Y. V. (2017). Oxygen

372   ions O^+ energized by kinetic Alfvén eigenmode during dipolarizations of intense substorms.

373   Journal of Geophysical Research: Space Physics, 122. https://doi.org/10.1002/ 2017JA024418

374   Ebihara, Y., M.‐C. Fok, T. J. Immel, and P. C. Brandt (2011), Rapid decay of storm time ring

375   current due to pitch angle scattering in curved field line, J. Geophys. Res., 116, A03218,

376   doi:10.1029/2010JA016000.

377   Fok, M., Moore, T. E., Brandt, P. C., Delcourt, D. C., Slinker, S. P., & Fedder, J. A. (2006).

378   Impulsive enhancements of oxygen ions during substorms. Journal of Geophysical Research, 111,

379   A10222, doi:10.1029/2006JA011839.

380   Frank, L. A., W. R. Paterson, and J. B. Sigwarth (2002), Observations of plasma injection into the

381   ring current during substorm expansive phase, J. Geophys. Res., 107(A11), 1343,

382   doi:10.1029/2001JA000169.

383   Fuselier, S. A., D. M. Klumpar, W. K. Peterson, and E. G. Shelley, Direct injection of ionospheric

384   O^+ into the dayside low latitude boundary layer, *Geophys. Res. Lett.*, *16*, 1121-1124, 1989.

385   Fuselier, S. A., D. M. Klumpar, and E. G. Shelley (1991), Ion reflection and transmission during

386   reconnection at the Earth's subsolar magnetopause, Geophys. Res. Lett., 18, 139–142,

387   doi:10.1029/90GL02676.

388   Fuselier, S. A., et al. (2016), Magnetospheric ion influence on magnetic reconnection at the

389   duskside magnetopause, Geophys. Res. Lett., 43,1435–1442, doi:10.1002/2015GL067358.

390   Fuselier, S. A., Trattner, K. J., Petrinec, S. M., Denton, M. H., Toledo‐Redondo, S., André, M.,

391   et al. (2019).Mass loading the Earth's dayside magnetopause boundary layer and its effect on

392   magnetic reconnection. Geophysical Research Letters, 46, doi:10.1029/2019GL082384.

393   Ganushkina, N. Y., Pulkkinen, T. I., & Fritz, T. (2005). Role of substorm-associated impulsive

394   electric fields in the ring current development during storms. Annales Geophysicae, 23(2), 579–

395   591, doi:10.5194/angeo-23-579-2005.

396   Hsu, T.‐S., and McPherron, R. L. (2003), Occurrence frequencies of IMF triggered and

397   nontriggered substorms, J. Geophys. Res., 108, 1307, doi:10.1029/2002JA009442, A7.

398   Kim, K. C., Lee, D.‐Y., Lee, E. S., Choi, C. R., Kim, K. H., Moon, Y. J., Cho, K. S., Park, Y. D.,

399   and Han, W. Y. (2005), A new perspective on the role of the solar wind dynamic pressure in the

400   ring current particle loss through the magnetopause, J. Geophys. Res., 110, A09223,

401   doi:10.1029/2005JA011097.

402   Keika, K., P. C. Brandt, M. Nosé, and D. G. Mitchell (2011), Evolution of ring current ion energy

403   spectra during the storm recovery phase: Implication for dominant ion loss processes, J. Geophys.

404   Res., 116, A00J20, doi:10.1029/2010JA015628.

405   Keika, K., L. M. Kistler, and P. C. Brandt (2013), Energization of O^+ ions in the Earth's inner

406   magnetosphere and the effects on ring current buildup: A review of previous observations and

407   possible mechanisms, J. Geophys. Res. Space Physics, 118, 4441–4464, doi:10.1002/jgra.50371.

408   Kronberg, E. A., Ashour-Abdalla, M., Dandouras, I., Delcourt, D. C., Grigorenko, E. E., Kistler, L.

409   M.,…Zelenyi, L. M. (2014). Circulation of heavy ions and their dynamical effects in the

410   magnetosphere: Recent observations and models. Space Science Reviews, 184(1-4), 173–235,

411   doi:10.1007/s11214-014-0104-0.

412   Lennartsson, W., & Shelley, E. G. (1986). Survey of 0.1- to 16-keV/ e plasma sheet ion

413   composition. Journal of Geophysical Research, 91(A3), 3061.

414   Li, X., M. Hudson, A. Chan, and I. Roth (1993), Loss of ring current O^+ ions due to interaction

415   with Pc 5 waves, J. Geophys. Res., 98, 215–231, doi:10.1029/92JA01540.

416   Liu, Y. H., C. G. Mouikis, L. M. Kistler, S. Wang, V. Roytershteyn, and H. Karimabadi

417 (2015),The heavy ion diffusion region in magnetic reconnection in the Earth's magnetotail,

418 J.Geophys. Res., 120, 3535-3551, doi:10.1002/2015JA020982.

419 Moore, T. E., Arnoldy, R. L., Feynman, J., and Hardy, D. A.: Propagating substorm injection

420 fronts, J. Geophys. Res., 86, 6713– 6726, 1981, doi:10.1029/JA091iA03p03061.

421 Nosé, M., Lui, A. T. Y., Ohtani, S., Mauk, B. H., McEntire, R. W., Williams, D. J.,…Yumoto, K.

422 (2000). Acceleration of oxygen ions of ionospheric origin in the near-Earth magnetotail during

423 substorms. Journal of Geophysical Research, 105(A4), 7669–7677, doi:10.1029/1999JA000318.

424 Ohtani, S., M. Nosé, S. P. Christon, and A. T. Y. Lui (2011), Energetic O^+ and H^+ ions in the

425 plasma sheet: Implications for the transport of ionospheric ions, J. Geophys. Res., 116, A10211,

426 doi:10.1029/2011JA016532.

427 Ono, Y., M. Nose, S. P. Christon, and A. T. Y. Lui (2009), The role of magnetic field fluctuations

428 in nonadiabatic acceleration of ions during dipolarization, *J. Geophys. Res.*, 114, A05209,

429 doi:10.1029/2008JA013918.

430 Phan, T. D., Dunlop, M. W., Paschmann, G. et al.: Cluster observations of continuous

431 reconnection at the magnetopause under steady interplanetary magnetic field conditions, Ann.

432 Geophys., 22, 2355–2367, 2004,

433 Sonnerrup, B. U. Ö., G. Paschmann, I. Papamastorakis, N. Sckopke, G. Haerendel, S. J. Bame, J.

434 R. Asbridge, J. T. Gosling, and C. T. Russell (1981), Evidence for magnetic field reconnection at

435 the Earth's magnetopause, J. Geophys. Res., 86, 10,049–10,067, doi:10.1029/JA086iA12p10049.

436 Slapak, R., H. Nilsson, L. G. Westerberg, and A. Eriksson (2012), Observations of oxygen ions in

437 the dayside magnetosheath associated with southward IMF, J. Geophys. Res., 117, A07218,

438 doi:10.1029/2012JA017754.

439 Slapak, R., Nilsson, H., Westerberg, L. G., and Larsson, R.: O+ transport in the dayside

440 magnetosheath and its dependence on the IMF direction, Ann. Geophys., 33, 301-307,

441 doi:10.5194/angeo-33-301-2015.

442 Wang, S., L. M. Kistler, C. G.Mouikis, Y. Liu, and K. J. Genestreti (2014), Hot magnetospheric

443 O^+ and cold ion behavior in magnetopause reconnection: Cluster observations, J. Geophys.Res.,

444 119, 9601-9623, doi:10.1002/2014JA020402.

445 Welling, D. T., Jordanova, V. K., Zaharia, S. G., Glocer, A., and Toth, G. (2011), The effects of

446 dynamic ionospheric outflow on the ring current, J. Geophys. Res., 116, A00J19,

447   doi:10.1029/2010JA015642.

448   Winglee, R. M., Lewis, W., and Lu, G. (2005), Mapping of the heavy ion outflows as seen by

449   IMAGE and multifluid global modeling for the 17 April 2002 storm, J. Geophys. Res., 110,

450   A12S24, doi:10.1029/2004JA010909.

451   Winglee, R. M., and Harnett, E. (2011), Influence of heavy ionospheric ions on substorm onset, J.

452   Geophys. Res., 116, A11212, doi:10.1029/2011JA016447.

453   Yau, A. W., and M. André (1997), Sources of ion outflow in the high latitude ionosphere, *Space*

454   *Sci. Rev.*, 80, 1.

455   Yau, A. W., A. Howarth, W. K. Peterson, and T. Abe (2012), Transport of thermal-energy

456   ionospheric oxygen (O$^+$) ions between the ionosphere and the plasma sheet and ring current at

457   quiet times preceding magnetic storms, *J. Geophys. Res.*, 117, A07215,

458   doi:10.1029/2012JA017803.

459   Yu, Y., and A. J. Ridley (2013), Exploring the influence of ionospheric O$^+$ outflow on

460   magnetospheric dynamics: dependence on the source location, J. Geophys. Res. Space Physics,

461   118, 1711–1722, doi:10.1029/2012JA018411.

462   Zong, Q.‐G., Wilken, B., Fu, S. Y., Fritz, T. A., Korth, A., Hasebe, N., Williams, D. J., and Pu,

463   Z.‐Y. (2001),Ring current oxygen ions escaping into the magnetosheath, J. Geophys.

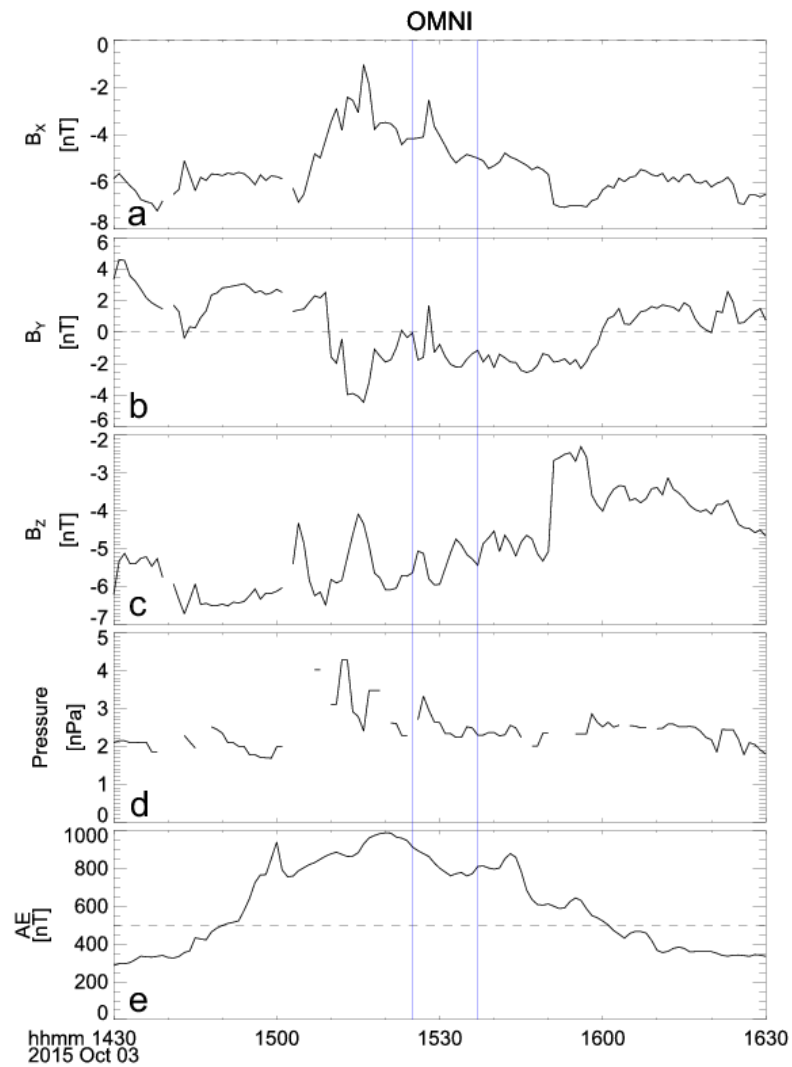464   Res., 106(A11), 25541– 25556, doi:10.1029/2000JA000127.

465

466
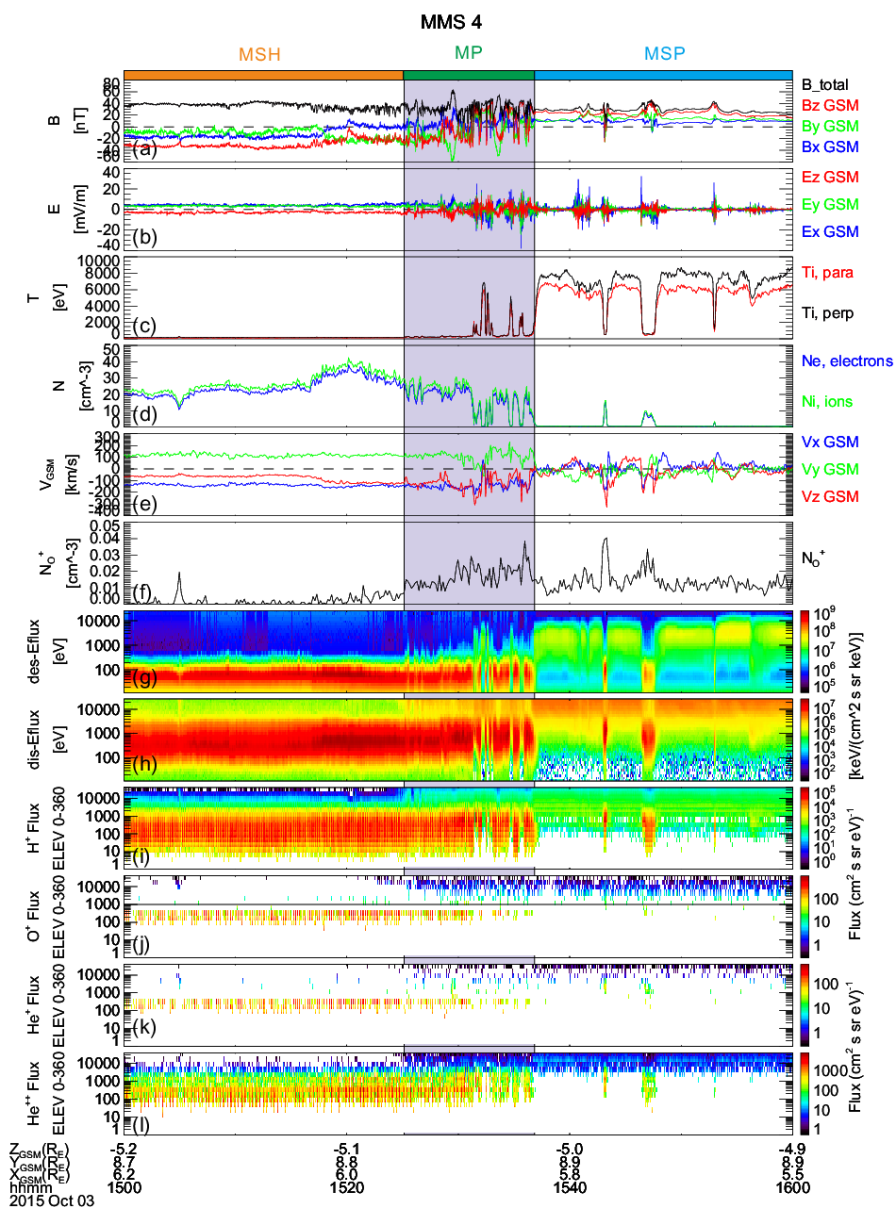
467

468

469   **Figures and Captions**

470

471   Figure 1. The IMF three components Bx,By, Bz, solar wind dynamic pressure and AE index from
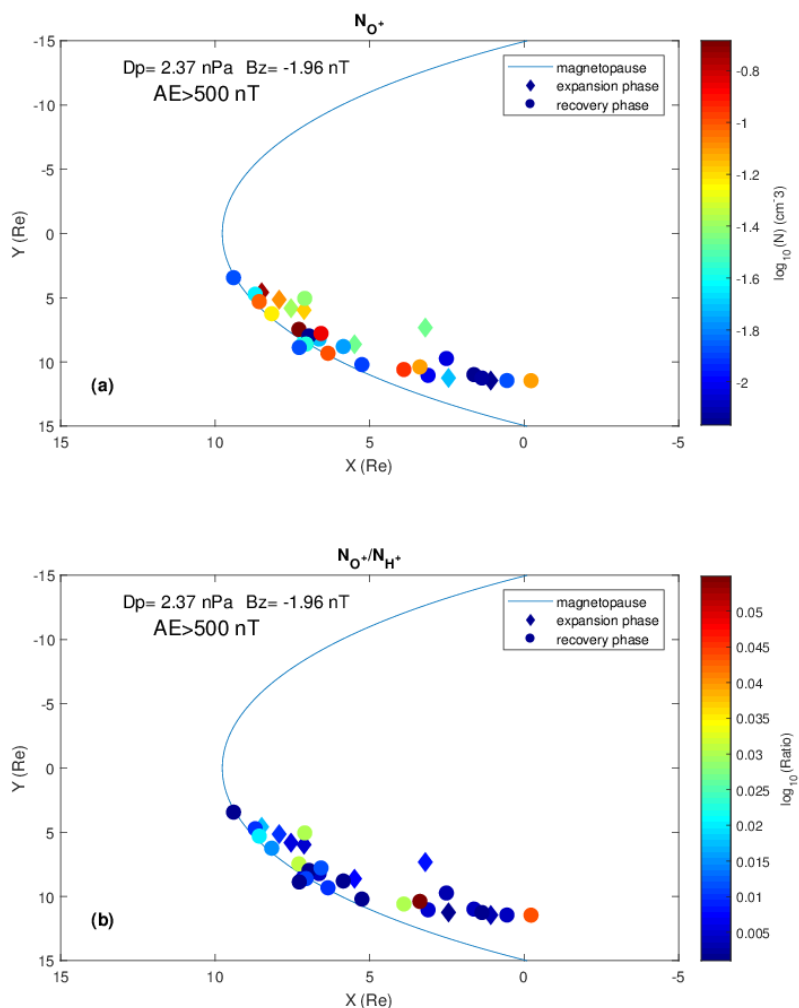
472   CDAweb OMNI data.

Figure 2. The energetic O$^+$ are observed at the magnetopause during an intense substorm on 03 October 2015 by MMS 4. From top to bottom are (a) the magnetic field three components, Bx (blue line), By (gree line), Bz (red line) and the total magnitude Bt (black line), (b) the electric field three components, Ex (blue), Ey (gree) and Ez (red), (c) Ion parallel (red) and

478   perpendicular(black) temperature, (d) The number density of ion (green) and electron (blue), (e)

479   three components of the ion velocity, (f) number density of O^+ (>1keV), (g) electron

480   omni-directional differential particle fluxes, (h) ion omni-directional differential particle fluxes,(i)

481   to (k) present omnidirectional differential particle fluxes of H^+, O^+, He^+, He^{++}, respectively. The

482   Geocentric Solar Magnetospheric (GSM) coordinate system is adopted. The thick bars at the top

483   of panel represent different regions encountered during this magnetopause crossing event. The

484   orange and blue bars represent the magnetosheath and the magnetosphere, respectively. The green

485   bar represents the magnetopause region. The FPI data in Figure 2(c-e) and (g-h) are in fast mode.
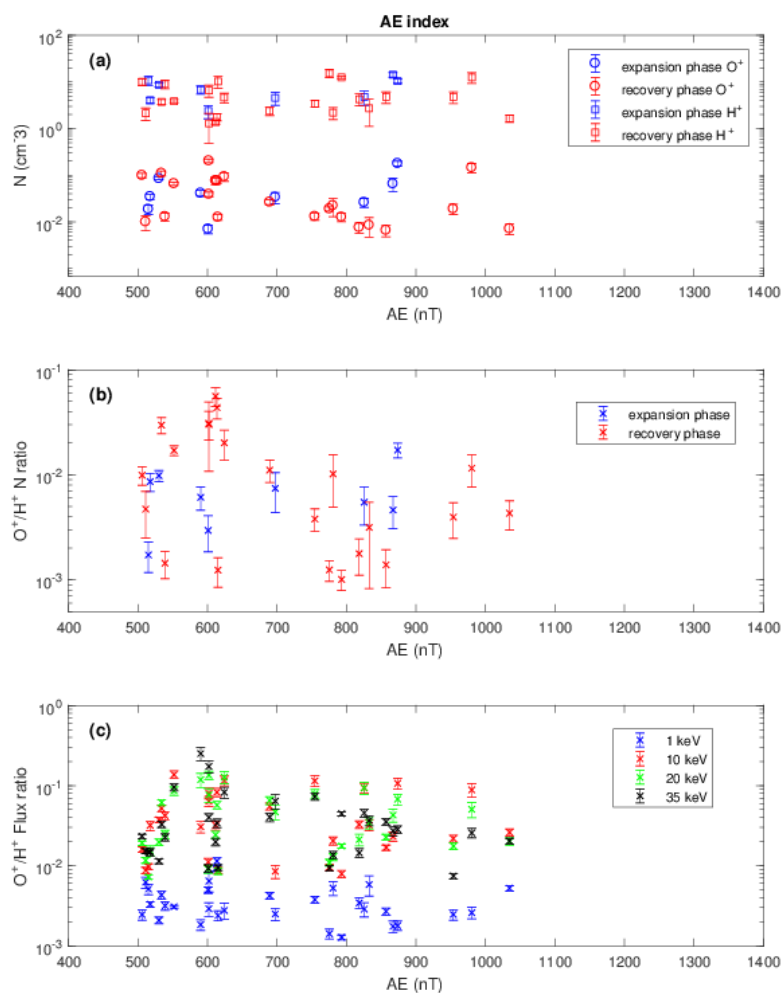
486

487

Figure 3. Maps of 31 events of energetic O^+ at the dusk flank magnetopause during intense substorms with AE index larger than 500 nT in XY_{GSM} plane. The O^+ number density and the number density ratios of O^+/H^+ are shown by the color signatures at the corresponding magnetopause location in Figure 3a and 3b, respectively. The blue curve line represents the
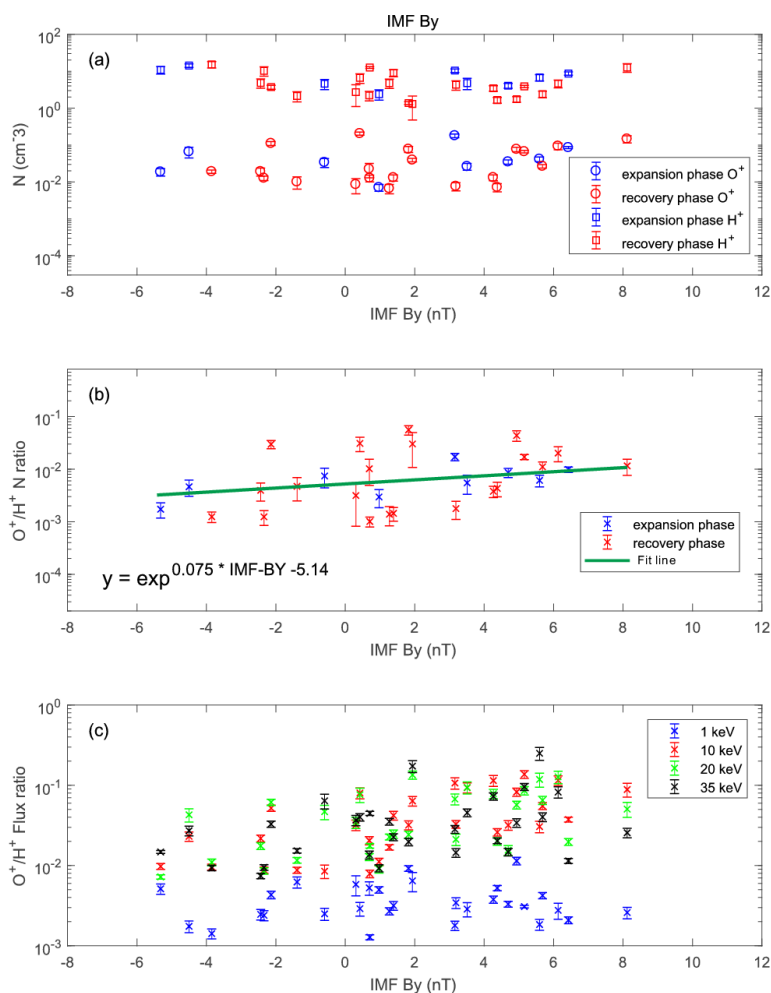
492   nominal magnetopause. The diamond and circle represent the event at the magnetopause during

493   the intense substorm expansion phase and recovery phase, respectively.
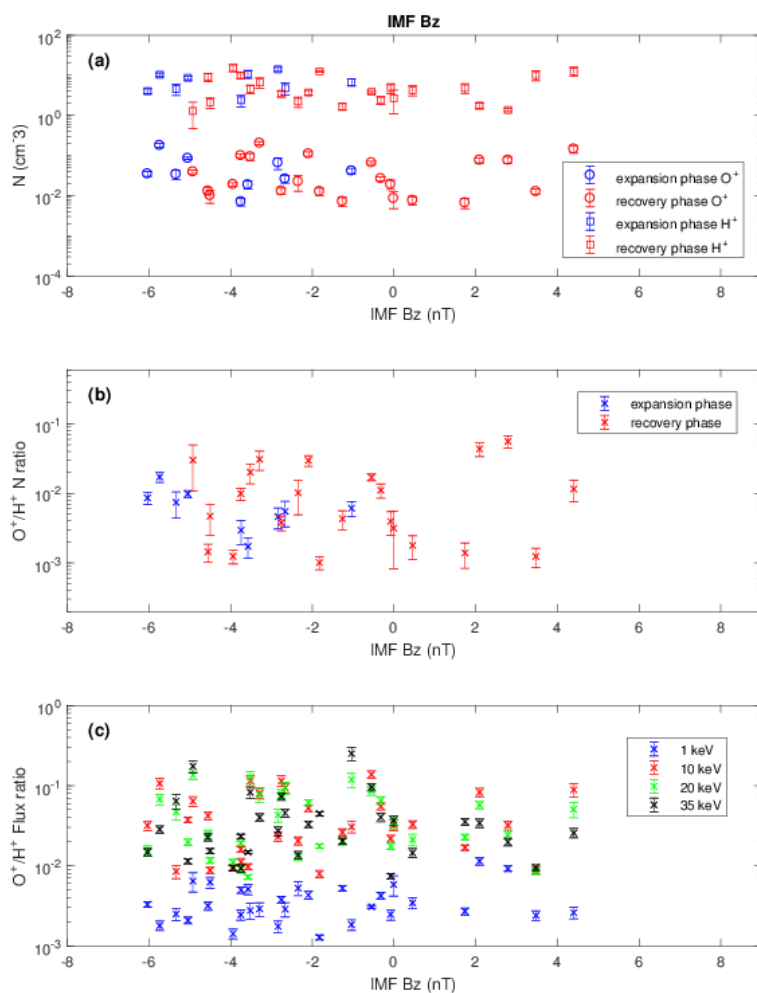
494

495

496   Figure 4. The relationship between the energetic O^+ at the dusk flank magnetopause and AE index

497   during intense substorms. From top to bottom, panels show that the O^+ and H^+ number density,

498   Figure 4a, the number density ratio of O^+/H^+, Figure 4b, and particle flux ration of O^+/H^+, Figure

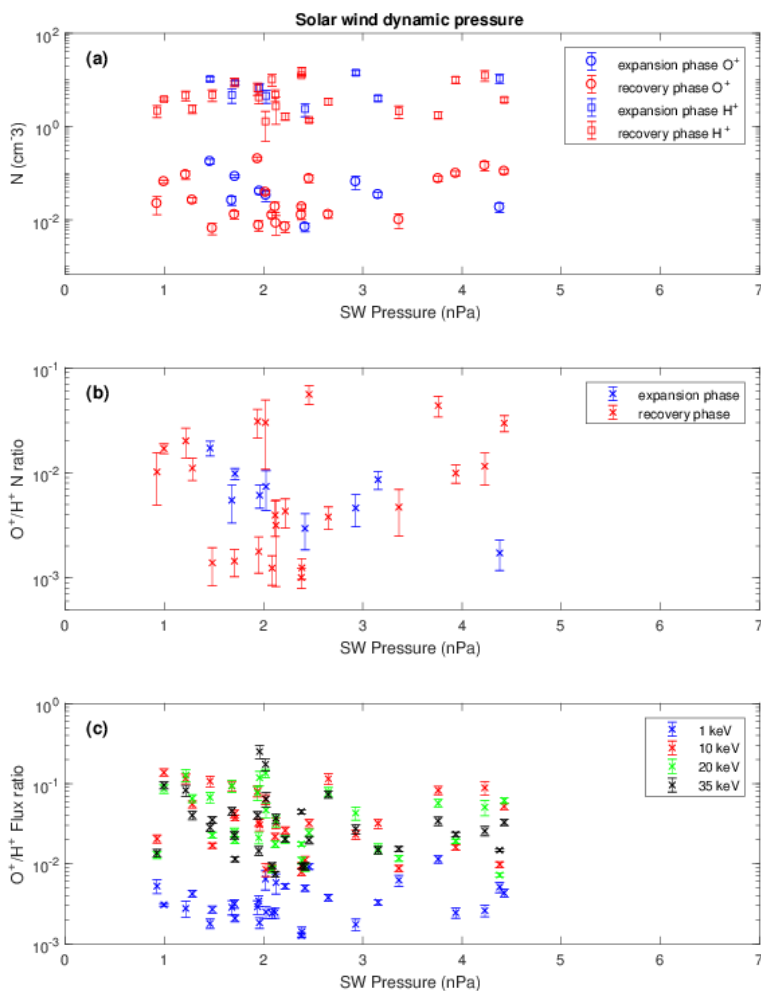499   4c, respectively. Error bars indicate 95% confidence intervals.

500

501

Figure 5. The relationship between the energetic O^+ at the dusk flank magnetopause and IMF By

during intense substorms. From top to bottom, panels show that the O^+ and H^+ number density,

Figure 5a, the number density ratio of O^+/H^+, Figure 5b, and particle flux ration of O^+/H^+ Figure

5c, respectively. The black line in figure 5b indicates a linear fit to the logarithm of O^+/H^+ number

density ratio. Error bars indicate 95% confidence intervals.

507

508

Figure 6. The relationship between the energetic O^+ at the dusk flank magnetopause and IMF Bz

during intense substorms. From top to bottom, panels show that the O^+ and H^+ number density,

Figure 6a, the number density ratio of O^+/H^+, Figure 6b, and particle flux ration of O^+/H^+ Figure

6c, respectively. Error bars indicate 95% confidence intervals.

513

Figure 7. The relationship between the energetic O^+ at the dusk flank magnetopause and solar wind dynamic pressure during intense substorms. From top to bottom, panels show that the O^+ and H+ number density, Figure 7a, the number density ratio of O^+/H^+, Figure 7b, and particle flux ration of O^+/H^+ Figure 7c, respectively. Error bars indicate 95% confidence intervals.